The IRAS2 and IRAS4 Outflows and Star Formation in NGC 1333

W. D. Langer[1], A. Castets[2], and B. Lefloch[2,3]

[1] MS 169-506, Jet Propulsion Laboratory, California Institute of Technology, Pasadena, CA 91109; langer@langer.jpl.nasa.gov

[2] Laboratoire d'Astrophysique, Observatoire de Grenoble, BP 53, F-38041, Grenoble Cedex 9, France; castets@gag.observ-gr.fr

[3] IRAM, Avda. Divina Pastora 7, N. C., 18012 Granada, Spain; lefloch@iram.es

Received ; accepted .

ABSTRACT

We report the first detection of the western bowshock component from IRAS2 in NGC 1333 along with observations of previously detected shocks and Outflow winds from this source and those from IRAS4. We compare the shock and outflow distributions from these two young stellar objects, and the locations of other YSOs, with the overall distribution of the dense molecular gas in the star forming core using high spatial resolution observations of CS (J = ? -], 3 - - 2, and 5 - - 4) emission made with L} IC]}{.-lll301,1 antenna. These comparisons provide a new picture of the morphology and dynamics Of the star forming core of NGC]333. The CS maps show: 1) a large cavity with many YSOs just at the inner edge of the cavity; 2) a, dense compressed shell at 8 km s-]; and, 3) a gas layer at 7 km S^{-1} probably located inside the cavity. We find that the IRAS2 and IRAS4 outflows impact different gas layers as indicated by the spatial association of the red and blue shifted lobes, and that IRAS2 is located near the front edge of the CS shell. The burst of star formation, which has shaped NGC 1 333, is occurring in the compressed shell traced by CS and now appears to be in a, late evolutionary stage.

Subject headings: ISM: individual (NGC1333); ISM: jets and outflows; ISM: molecules - stars: formation

1. INTRODUCTION

NGC 1333 is a star forming core in Perseus whose structure is strongly influenced by embedded young stellar objects (YSOs), which are visible mainly in the infrared. Lada, Alves & Lada (1996) estimate that a burst of star formation is taking place here at 5×10^{-5} $M_{\odot}$ per year. Our moderate resolution ^{13}CO, $C^{18}O$ (100″) and CS (120″) study (Warin et al. 1996) revealed the existence of a cavity in the cloud's center. Many infrared and outflow sources (SSV 12 and 13, IRAS2, and IRAS4) appear to be associated with this cavity. IRAS4 is a class '0' source originally studied in the submillimeter continuum by Sandell et al. (1991) and in molecular emission by Blake et al. (1994). It is a binary system with two components separated by 30″ (IRAS-4A and IRAS-4B). IRAS2 has been studied by Jennings et al. (1987) and Sandell et al. (1994) who detected a shock associated with the eastern outflow from IRAS2 at the edge of the cavity. Recent SiO and CS interferometric observations (Blake & Mundy 1996) clearly show the bowshocked gas here. In Warin et al. we suggested that some of these outflows were responsible for creating the cavity and forming a compressed shell of gas at its boundary with the core. However, these observations barely resolved the cavity, and did not resolve the surrounding shell, outflows, and shocks. To investigate in more detail the structure and dynamics of the cavity, shell, and the sources responsible for these structures we undertook a large scale CS multi-transition, high spatial resolution map of this region using the IRAM 30m antenna in Pico Veleta, near Granada, Spain. We chose CS because it is a good probe of high density gas. In this *Letter* we bring together the radio and infrared observations to analyze the relationship between the size and shape of the cavity, the location of the sources, and the influence of outflows and shocks on the structure of the cloud. We also detected new shocks around IRAS4 and IRAS2, which also appear to influence the shell structure. The location of the YSOs and direction of the outflows indicated that the core of NGC 1333 may be undergoing sequential

star formation driven bipolar winds sweeping up material and shock compressing the gas.

2. OBSERVATIONS

Our results are based on simultaneous observations of the CS molecule in three transitions, J= 2→1, 3→2, and 5→4 made in September 1995 with the IRAM 30m telescope. The weather was always stable and clear during the observations. The three SIS receivers were calibrated by inserting two different temperature loads. All the receivers were connected to the same backend, an autocorrelator split into three parts. The spectral resolution was about 0.10 $km\,s^{-1}$ and the HPBW was 25″, 16″, and 10″ at 98, 147, and 245 GHz, respectively. Most of the data were obtained using the frequency switching mode with a shift of 7.7 MHz for the 2 and 3mm receivers and 15.4 MHz for the 1 mm receiver. We used the position switching mode ill and around the bow shocks and outflow sources to increase the velocity coverage (off position: RA = 15′ and DEC = 6′ about the center). We mapped on a uniform 24″ grid in the cloud and every 12″ around the shocks and outflow sources. All offsets refer to the center of the map (SSV13) situated at $\alpha(1950)$, $03^h25^m57.4^s$ and $\delta(1950)$: 31 °05′49″. The full CS map covers 420″ in RA and 620″ DEC. For receiver calibration several known sources were monitored regularly during the course of the observations. The pointing accuracy was checked every two hours on planets or continuum sources and was better than 3″. The spectra were corrected for beam efficiency and all intensities are given in units of mainbeam brightness temperature

3. RESULTS

In Figure 1 we show our CS(3→2) intensity map, integrated over the entire velocity range, including the line wings (the lower resolution CS(2→1) map is similar). The cavity is

clearly resolved in this image and is 'pear' shaped, oriented roughly N-S, measuring 260″ in DEC and 140″ in RA in the south. In the high spatial resolution CS maps the edge of the cavity is very sharp indicating a large density gradient. We have superimposed on the CS map the near infrared (NIR) excess sources observed by Aspin et al. (1994) together with additional NIR excess sources recently detected by Lada et al. (1996). These sources seem good candidates for PMS stars deeply embedded in the NGC1333 molecular gas. First, several of the sources with infrared excess, such as SSV10-13 and IRAS2, are located in the shell. These are very young stars which are obviously still embedded in their parental gas and thus the CS shell seems to be an active site of star formation. Second, there are several sources in the cavity and many of these are located just at the boundary of the shell (within 20″ of the edge). The sources in the cavity are likely candidates for clearing out the region and shaping the cavity. Third, very notable in the south are several localized peaks in CS(3-→2) (and 2-→1) integrated intensity. Two of these appear to be associated with SSV13 and IRAS4, one is associated with the SSV13 outflow (tracing the HH7-11 Herbig-Haro objects), and another corresponds to the eastern bowshock associated with IRAS2 (Sandell et al. 1994). In addition, there is another feature to the west of IRAS2, not seen before, which we will argue in the following section is a bowshock arising from the IRAS2 outflow.

3.1. IRAS4 and IRAS2

There are several velocity components evident in the CS spectra. In most places we observe two well separated narrow gaussian lines which trace two layers of ambient gas one at V_{lsr} around 7 km s^{-1} and another at 8 km s^{-1}, having line widths $\sim$ 1.1 km s^{-1}. In the neighborhood of IRAS4, we also observe high velocity line wings that we identify as the outflow generated by IRAS4 (cf. Blake et al. 1995). In figure 2a we show the CS spectra at the location of IRAS4A (offset: 108″, -156″). A high velocity wing is very apparent in the

feature is seen in CS(2-›1) but not in CS(5-›4) and also at IRAS2E in all 3 CS transitions). At the location of the IRAS2 eastern and western outflows the center velocity of this shocked gas changes very rapi dly as we move along the axis of the outflow (Figure 2b). At offset (-21 6", -72") only the ambient gas ($\Delta V \sim$ 1 km s^{-1}) is present, yet within 12" the shocked gas is evident as seen at (-204",- 72") in Figure ?, where it peaks at $V_{lsr} \sim 1$ km s- ^{1} and has a line width about 7 km s^{-1}. The peak in the spectrum of the shocked gas shifts to about 2.5 km s^{-1} at (-1 92'', -7'2") and reaches a maximum shift of 6.5 km s^{-1} at (-144", -'72"), the eastern-most edge of the shocked region. The large velocity gradient at the western edge is characteristic Of the leading edge of a shock where the ambient gas is undergoi ng acceleration. We estimate that the maximum velocity gradient is equal to 150 km s^{-1}pc^{-1}at (-l S6", - 72"). The CS spectra of the eastern bow-shock IRAS2E show both ambient components and the shock emission. In our CS(3-›2) map (Figure 4) the eastern bow-shock extends over 40" by 30" in RA and DEC, respectively. The shock emissio n overlaps the 8 km s^{-1} componen t making it difficult to quantify the line paramet ers.

In the CS(3-›2) and (2-›1) maps the '[km s^{-1} component has an unusual velocity distribution. The line peak velocity is constant ($V_{lsr} \sim 7.2$ krn s^{-1}) over much of the map except at two locations where it is much lower, $\sim$ 6.5 km s^{-1}. One Of these is close to the end of the red IRAS2 eastern outflow and the other is situated at the end of the blue IRA S4A outflow. The region at the end of the IRAS2 red lobe (IRAS2E) is a, known shocked region accompanied by an increase in the density of the ambient gas (Sa n dell et al. 1994). That these "velocity holes" are exa ctly situated in the end Of the molecular outflows is certai nly not accidental, but is probably rela ted to the shock. Additional observations are needed to clarify this point. The spatial map of (; (3-›2) intensity integrated only over t h e 7 km s^{-1} layer (not shown), reveals that these interaction regions between the outflows and the ambient molecular gas sit in the 7 km s^{-1} layer. Furthermore, the map of the two outflow lobes driven by IRAS4 shows that it is the blue lobe which is impacting onto the '7

km s^{-1} layer. Therefore the 7 km s^{-1} layer lies in front Of the 8 km s^{-1} one

3.2. Excitation Conditions

We used the three CS transitions along with an LVG excitation model to estimate the density, $n(H_2)$, and column density, N(CS), Of the gas components adopting the collisional excitation rates of Green & Chapman (1978). The line parameters were derived by fitting a gaussian to each component. When an outflow wing was present, as at (1 08", -1 56") in figure 2a, we subtracted its contribution to the ambient line using a polynomial extrapolation of the outflow wing over the velocity width of this line. The hardest case to fit is where the shocked material is nearly blended with the cloud component (e.g. IRAS2E bow-shock). Here we extracted the ambient line parameters for the cloud assuming the same linewidth as in the nearby spectra and a gaussian shape for the shocked emission line. It was impossible to fit all three transitions self-consistently and also determine the kinetic temperature. This inconsistency suggests that the bulk of the CS(5-›4) emission may be coming from the shocked gas at the V_{lsr} of the ambient components and hence that it is difficult to determine the correct 5-›4 intensity to use for the excitation analysis of the ambient gas. Therefore we used only the CS(3-›2) and (2-›1) transitions, assuming a kinetic temperature of 20K (Warin et al.). Typical solutions are given in Table 1 and summarized here. (1) $n(H_2)$ and N(CS) in the two layers are fairly uniform and on average $\sim 2 \times 10^5$ cm^{-3} and 2×10^{13} cm^{-2}, respectively. These values increase slightly at IRAS2E perhaps indicating the presence of a denser core. (2) The CS(5-›4) emission seems to come mainly from the shocked gas, except in the 7 km s^{-1} layer near IRAS2E, where a consistent three transition solution can be found if $T_k = 40$K. (3) Sandell et al. gave $N(CS) \sim 1.4 \times 10^{14}$ cm^{-2} for the red shifted high velocity gas in the East bow shock assuming that CS is optically thin and thermalized at 7.5 K. We believe their value of N(CS) is too high

because they did not subtract the cloud component. They also say that the dip in their CS(5-›4) spectrum may be due to residual CS emission in the reference p osition although they apparently did not verify it. We believe, instead, that their spectral shape is due to overlap of the two ambient components. We also calculated conditions in the warmer, presumably shocked, part of the gas using only CS(5-›4) and (3-›2). Representative results are given in Table 1 using T_k = 40 K. The densities usi ng CS(5-›4) are much higher than those obtained with CS(2-›1) and (3-›2), however N(CS) is still $\sim$ 1-? $\times 10^{13}$ cm^{-2}. Near IRAS4A, at (96″, -156″) in the 7 km s^{-1} layer, n(H_2) $\simeq$ 8 x 10^5 cm^{-3}, and N(CS) $\simeq$ 2 X 10^{13} cm^{-2}, close to those estimated by Blake et al. (1995). Thus the IRAS2E 'i km s^{-1} layer at the shock location shows, as expected, a density enhancement.

4. DISCUSSION

The derived physical conditions presented above and the locations of the YSOs suggest a new pict ure of the structure and dynamics of the star forming core of NGC] 333. The hig h resolution CS maps show a shell of dense gas, n(H_2) $\sim$ 2 x 10^5 cm^{-3}. Comparison with recent near- and far-IR observations (Aspin et al.; Lada et al.) show many YSOs just at the inner edge of the cavity. The south ern half of the NGC 1333 core appears to be composed of two gas layers with velocities that diffe r by at most] .2 km s^{-1} and which merge into a single broad feature to the south of SSV13 (Figure 4). The 8 km s^{-1} gas component exists almost everywhere in the maps, while the '[km s^{-1} one is only located in the south (RA ' '200" to -]()()" and DEC = -240″ to -50″). In order for IRAS2 to have its reel outflow impact the 7 km s^{-1} gas layer and its blue flow the 8 km s^{-1} gas layer, while the opposite is true for 1RAS4, these sources must be located on opposite sides of the 7 km s^{-1} layer. This indicates that the '(km s^{-1} layer is probably located in the middle of the cloud inside the cavity. Due to the position of the 'i' km s^{-1} layer, this pattern indicates that IRAS2 is

located near the front edge of the CS shell.

Only one of the infrared excess sources in Lada et al.'s sample, IRAS2, is found deep inside the high column density region which forms the southern part of the dense shell. Most of the others including SSV13 are either at the edge of this region, or in the lower column density western shell or in the cavity (see fig 1). Thus only IRAS4 and IRAS2 are embedded in the southern shell or core and these 2 sources are among the youngest sources in the cloud as evidenced by their SED class and CO outflows. The outflows from IRAS2 and IRAS4 may be part of the pattern of sequential star formation in NGC 1333 whereby each generation of stars produces shocks which compress the ambient gas and produce the next stage of star formation. The evidence for compression comes from our analysis of the CS (5- ›4) and (3- ›2) emission in the IRAS4A and IRAS2E region. The gas densities there are $\sim$ 1-4 $\times$ 10^6 cm^{-3}, about an order of magnitude larger than in the uncompressed regions. We speculate that, once the first stars form deep inside the cloud core they begin to dig out the cavity and compress the surrounding gas triggering the next star generation. This second generation enlarges the bubble and compresses the gas further forming a shell. That the relative positions of the young infrared excess sources seen by Lada et al. are mostly at the edge of the shell and some of the NIR sources of Aspin et al. are in the cavity would seem to favor this scenario. (It is not clear if IRAS4 fits into this picture because, although clearly very young, it is far away from the edge of the cavity. Possibly it has formed independently in a dense sub-fragment of the original cloud core.) However, to test this suggestion of sequential star formation we need additional observations (infrared spectroscopy, mid-infrared photometry) to characterize stellar age as a function of position.

We thank the IRAM telescope staff for their help and G. Blake and C. Lada for useful comments. WDL's research was made at the Jet Propulsion Laboratory, California Institute of Technology, under contract with the National Aeronautics and Space Administration.

Table 1: NGC 1333 Line Parameters and Physical Properties from CS

Region	$(\Delta\alpha, \Delta\delta)$	A v	V_{lsr}	$T_{mb}(2\text{-}1)$	$T_{mb}(3\text{-}2)^a$	$T_{mb}(5\text{-}4)^b$	n(H_2)	N(CS)
	(″,″)	kms^{-1}	kills-*	K	K	K	cm^{-3}	cm^{-2}
IRAS4A	(96,-156)	1.1	8.2	2.3	1.9		2.1(5)	1.3(13)
	(96,-156)	1.1	6.6	4.6	4.3		2. s)(3)	2.4(13)
IRAS2E	(0,-108)	0.9	s.]	2.7	2.8		4.4(5)	1.1(13)
	(0,-10s)	1.2	6.8	3.8	3.8		3,'1(5)	2.2(13)
	(-24, -10s)	1.2	s.1	2.1	2.3		5.0(5)	1.1(13)
	(-2?4,-10s)	0.9	6.6	7.0	6.5		2.7(5)	4.1(13)
IRAS2	(-120,-96)	1.2	8.0	3.0	2.5		2.2(5)	1.s(13)
	(-12? 0,-96')	1.2	7.0	2.0	1.5		1.7(5)	1.1(13)
IRAS2W	(-216, -7'2)	1.1'	7.9	2.4	1.7		1.4(5)	2.0(13)
	(-192,-72)	1.4	"(.i	2.4	2.0		2.1 (5)	1.5(13)
C1OLI(I	(0,-168)	0.9	7.8	2.9	2.8		3.1(5)	1.2(13)
	(0,-168)	1.0	6.9	4.3	3.6		1.9(5)	2.3(13)
IRAS4A	(96,-156)	1.1	8.2		1.9	1.7	1.6(6)	6.6(12)
	(96,-156)	1.1	6.6		4.3	2.7	8.0(5)	1.6(13)
IRAS2E	(-1?, -108)	1.1	s.]		2.2	1.7	1.2(6)	"(.5(12)
	(-1?, -108)	1.0	6.6		5.0	1.9	3.6(5)	1.9(13)
	(-24,-108)	1.1	8.1		3.7	3.9	2.3(6)	1.4(13)
	(-24 ,-1 08)	1.0	6.6		8.8	4,3	4.3(5)	3.8(13)

[a] The (3-›2) data has been degraded to the (2-›1) resolution for use with the (2-›1) data and we adopt T_k = 20 K.

[b] The (5- ›4) data has been degraded to the (3- ›2) resolution for use with the (3- ›2) data and we adopt T_k = . 40 K.

REFERENCES

Aspin, C., Sandell, G., & Russell, A. P. G. 1994, A&A Sup, **106**, 165

Blake, G. A., Sandell, G., van Dishoeck E. F., Groesbeck, T. D., Mundy, L. G. & Aspin, C. 1995, ApJ, **441**, 689

Blake, G. & Mundy, L. 1996, to be submitted to ApJ

Green, s, & Chapman, S. 1978, ApJS, 37, 169

Jennings, R. E., Cameron, D. M. H, Cuddle, W, & Hirsute, C. J. 1987, MNRAS, 226, 461

Lada, C. J., Alves, J., Lada, E. A. 1996, A pJ, in press.

Sandell, G., Aspin C., Duncan, W. D., Russell, A. P., & Robson E. I. 1991. ApJ, 376, L17

Sandell, G., Knee, L. B. G., Aspin, C., Robson, I. E., & Russell, A. P. G. 1994, A&A, 285, L1

Warin S., Castets A., Langer W. D., Wilson R. W., & Pagani, L., 1996, A&A, **306**, 935

This manuscript was prepared with the AAS LaTeX macros v3. O.

Fig. 1.- A contour map of the CS(3- ›2) emission in NGC 1333 integrated over all velocities (-5 to +14 km s^{-1}) made with the IRAM 30m antenna. The (0,0) position corresponds to the location of SSV13, $\alpha(1950) = 03^h25^m57.4^s$ and $\delta(1950) = 31°05'49''$ and the upper and right hand scales are offsets in arcsec. The stars indicate IRAS2, IRAS4A, IRAS4B, and SSV13 while the filled squares indicate all the other SSV and IRAS sources. The filled triangles are the near infrared excess sources from Aspin et al. (1994) and the empty triangles indicate additional NIR excess sources detected by Lada et al. (1996). The sources from Aspin et al. correspond to all entries noted NO and C_B in the "Consistent reddening" column of their table 5.

Fig. 2.- (a) In the left panel are the three CS transitions observed at the position of IRAS4A (located 5 arcsec to the west of the position given by Sandell et al. (1991)). The maximum emission is observed 12" to the west of our position. (b) In the right panel are the four CS(3- ›2) spectra observed at a declination of -72" along an east-west direction, corresponding to the IRAS2 west bow shock.

Fig. 3.- Position-velocity diagram for the CS(3- ›2) along the IRAS2 East-West outflow. The offset $\Delta\delta = 0$ corresponds to the IRAS2 position while -100 and +70 correspond to the western (IRAS2W) and eastern (IRAS2E) bowshock, respectively. Intensity levels go from 0.3 K to 5.7 K by 0.3K. Note the presence of the two narrow line ambient layers of gas at $\simeq$ 7 and 8 km s^{-1} and the sudden decrease in the velocity of the 7 km s^{-1} layer at the location of the eastern bowshock (see text).

Fig. 4,- Channel maps of CS(3- ›2) emission primarily of the ambient gas every 0.5 km s^{-1} from 6.0 to 9.5 km s^{-1}. Contours go from 0.4 to 5 by 0.4 K km s^{-1}. The 7 km s^{-1} component is located in the south and merges into the larger 8 km s^{-1} layer near SSV13. Channels containing only high velocity gas (from -8 to 5 and from 10 to 15 km s^{-1}) have been dropped to make the figure clearer.

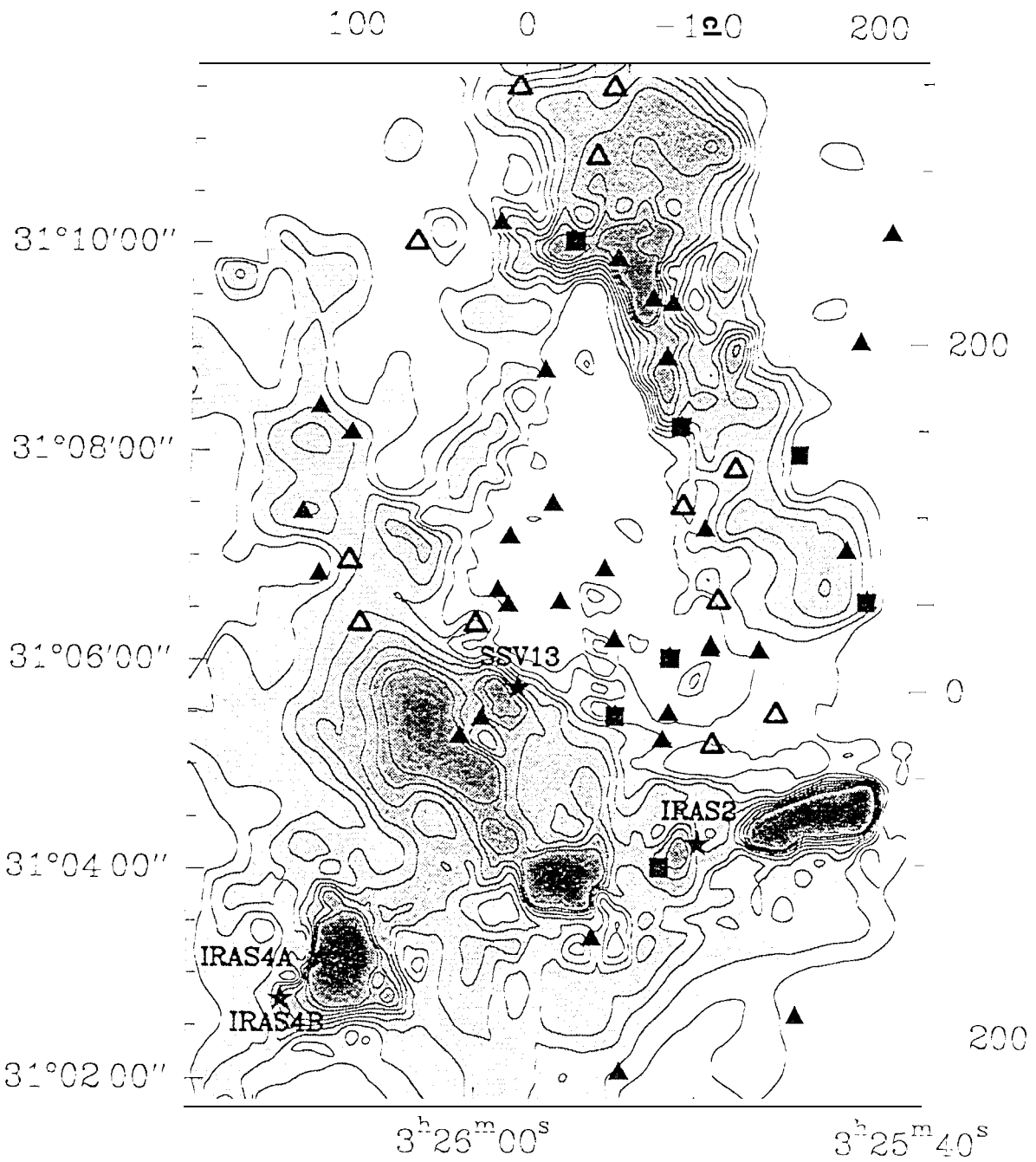
100
0
−100
200
31°10′00″
31°08′00″
31°06′00″
31°04′00″
31°02′00″
200
0
200
SSV13
IRAS2
IRAS4A
IRAS4B
3h26m00s
3h25m40s

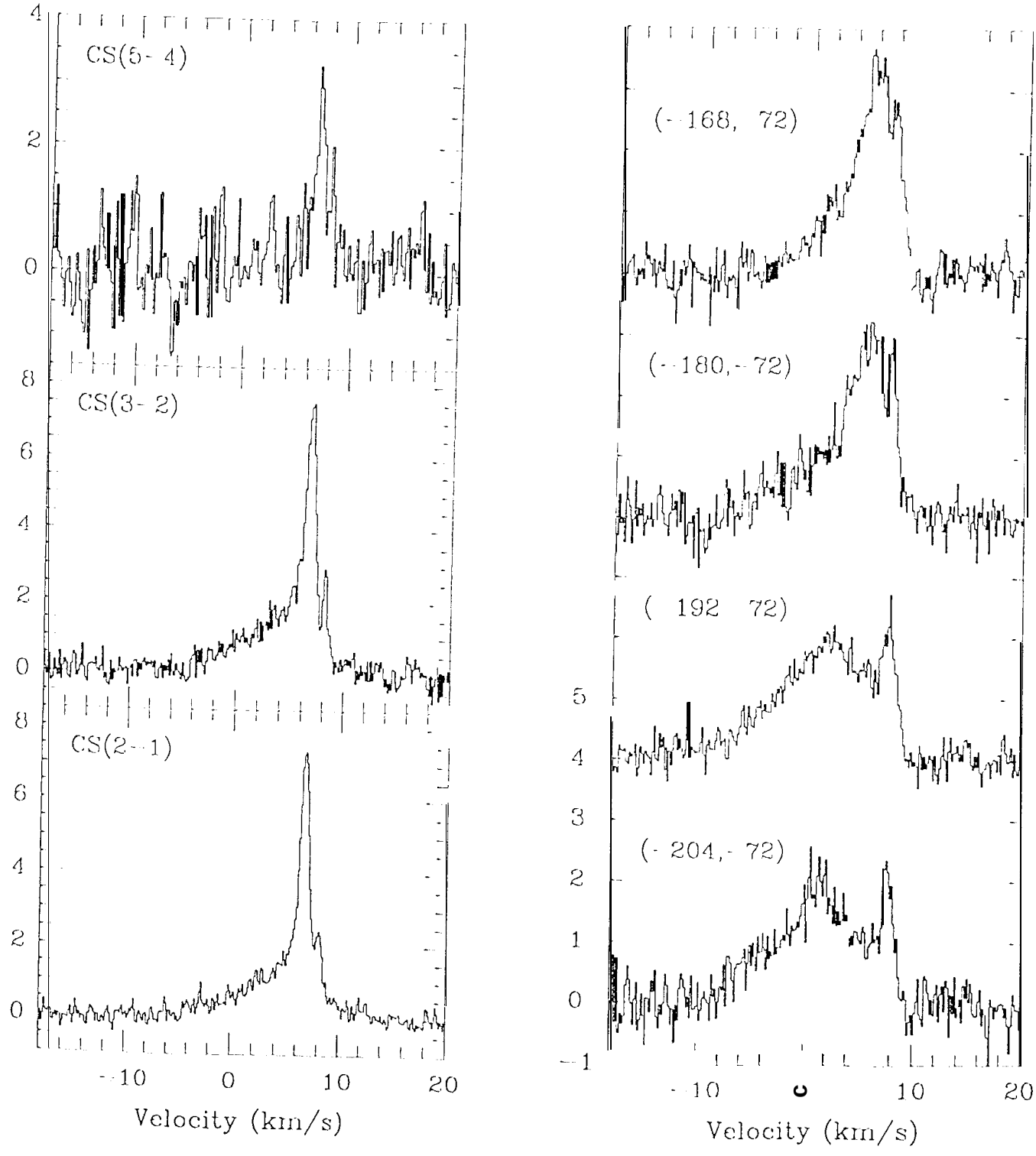
CS(5- 4)
CS(3- 2)
CS(2--1)
Velocity (km/s)
(- 168, 72)
(--180,-- 72)
(192 72)
(- 204,- 72)
Velocity (km/s)

Figure 2

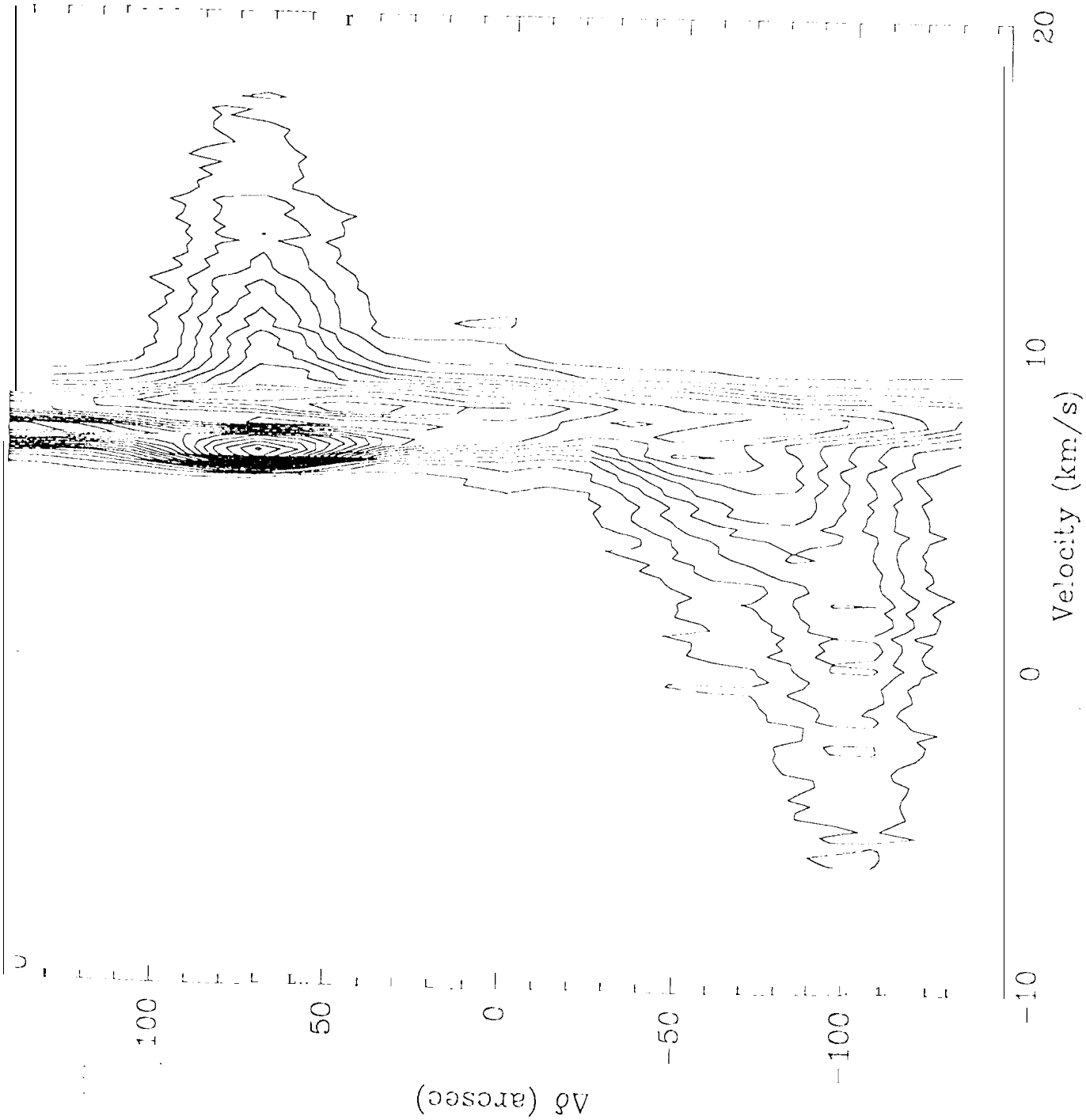

Figure 3

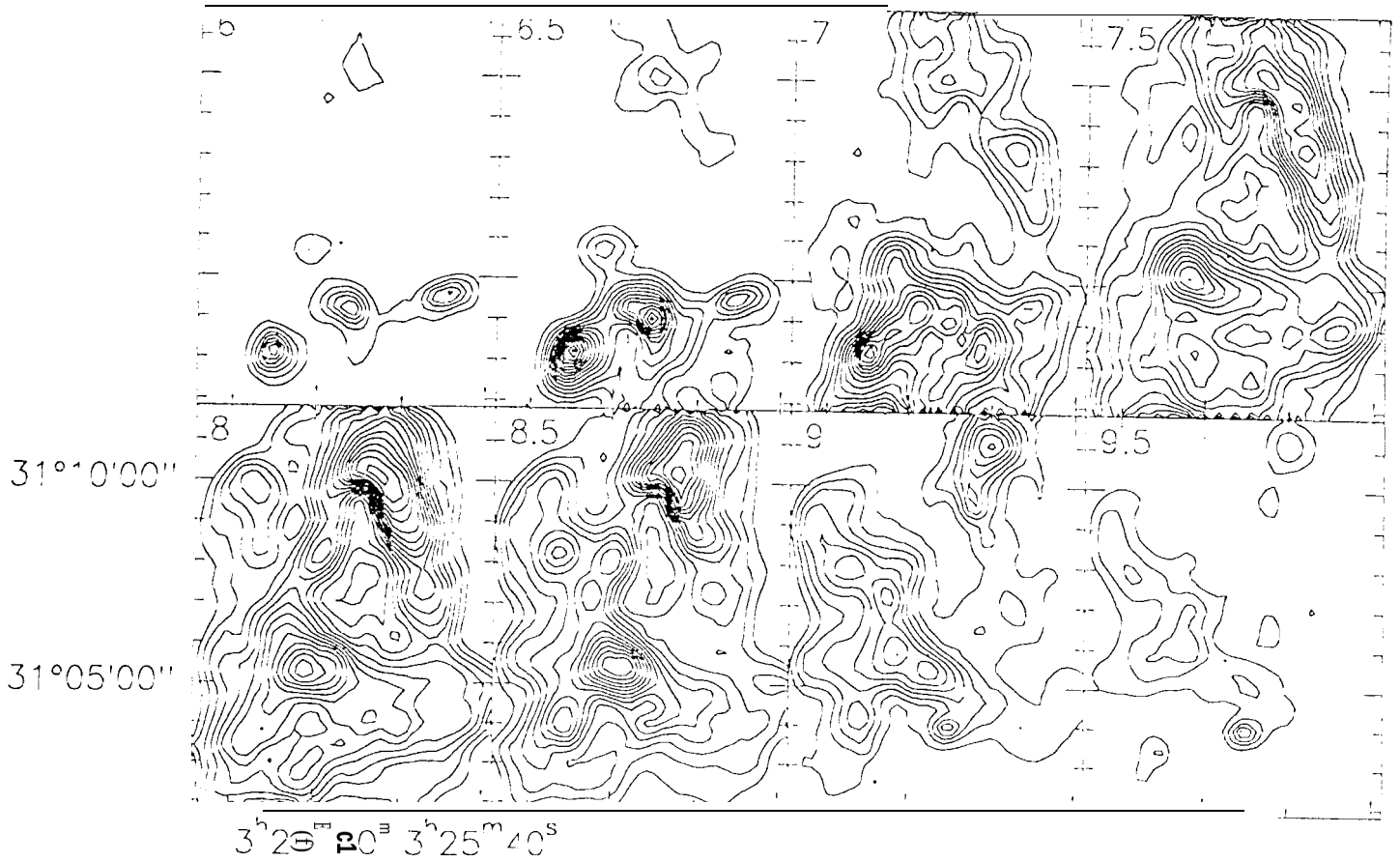

Figure 4